applied optics

Determination of optical constants of thin films in the EUV

Richard Ciesielski,[1,*] Qais Saadeh,[1] Vicky Philipsen,[2] Karl Opsomer,[2] Jean-Philippe Soulié,[2] Meiyi Wu,[2] Philipp Naujok,[3] Robbert W. E. van de Kruijs,[4] Christophe Detavernier,[5] Michael Kolbe,[1] Frank Scholze,[1] and Victor Soltwisch[1]

[1]Physikalisch-Technische Bundesanstalt, Abbestraße 2-12, 10587 Berlin, Germany
[2]imec, Kapeldreef 75, 3001 Leuven, Belgium
[3]optiX fab GmbH, Hans-Knöll-Str. 6, 07745 Jena, Germany
[4]MESA+, Institute for Nanotechnology, University of Twente, The Netherlands
[5]Ghent University, Department of Solid State Sciences, Krijgslaan 281/S1, 9000 Ghent, Belgium

*Corresponding author: richard.ciesielski@ptb.de

Received 29 October 2021; revised 13 January 2022; accepted 14 January 2022; posted 18 January 2022; published 8 March 2022

The determination of fundamental optical parameters is essential for the development of new optical elements such as mirrors, gratings, or photomasks. Especially in the extreme ultraviolet (EUV) and soft x-ray spectral range, the existing databases for the refractive indices of many materials and compositions are insufficient or are a mixture of experimentally measured and calculated values from atomic scattering factors. Since the physical properties of bulk materials and thin films with thicknesses in the nanometer range are not identical, measurements need to be performed on thin layers. In this study we demonstrate how optical constants of various thin film samples on a bulk substrate can be determined from reflection measurements in the EUV photon energy range from 62 eV to 124 eV. Thin films with thickness of 20 nm to 50 nm of pure Mo, Ni, Pt, Ru, Ta, and Te and different compositions of Ni_xAl_x, PtTe, Pt_xMo, Ru_xTa_x, Ru_3Re, Ru_2W, and TaTeN were prepared by DC magnetron sputtering and measured using EUV reflectometry. The determination optical constants of the different materials are discussed and compared to existing tabulated values.

https://doi.org/10.1364/AO.447152

1. INTRODUCTION

The complexity of functional nanostructures is constantly increasing in the semiconductor industry, and a key enabler for upcoming technologies beyond the 10 nm semiconductor node is new materials. Specifically, metals such as Pt, Te, Mo, and Ru start to play a central role as absorber materials in photolithography, for capping layers or as a means of thermal or electric contacts [1–4]. Their alloys are used to tune the material's properties to the desired values and therefore must be studied beforehand, which highlights the need for a precise and reliable determination of the physical constants of those thin film materials.

The precise measurement of optical properties in the extreme ultraviolet (EUV) regime around 91.85 eV/13.5 nm is still a challenge for the development of optical components such as photomasks or mirrors for EUV lithography [5–7]. Due to the short wavelength in this spectral regime, contamination, oxidation, or surface roughness in the nanometer range will affect the optical response of a sample much stronger than, for instance, at optical wavelengths. Such effects can be the result of chemical processes or contamination by process gases during the manufacturing or just a consequence of the grain structure of thin film samples. The most important material property for optical applications is the complex refractive index $\tilde{n} = n + ik = 1 - \delta - i\beta$, which, in the EUV and x-ray regime above 10 eV, is typically given in terms of δ, describing the dispersion, or refractive power, and β, describing the extinction of the incident radiation. Since the real part $n = 1 - \delta$ of refractive index $\tilde{n}$ is generally close to 1 and the imaginary part $k = -\beta$ is relatively large, the design of optical components for EUV applications is nontrivial [8,9]. An estimation of the optical properties of compound materials can be retrieved from the well-established representation in the form of atomic scattering factors [10], but it is not to be confused with actual spectral measurements of the optical constants. Here, a typical challenge is that the mass density of the compound materials is not known for the deposited thin films, which impacts the refractive index strongly. Thin film samples typically have a lower density than bulk samples, which is due to their more poly- and nanocrystalline structure, and due to more prominent surface effects. These effects are hard to predict, especially for compound materials. The most common way to determine optical constants in the x-ray range is through transmission experiments, which measure the absorption of the radiation directly [11]. Using the Kramers–Kronig relation, the complex refractive index can be determined from a measurement of the absorption. Since the penetration depth in the EUV regime is very low, ultra-thin and freestanding films are required for this type of measurement, which has an impact on the accuracy. Another major problem for transmission mode measurements is that the optical properties extracted from freestanding thin films are not always identical to thin layers within stratified systems as they are used in optical components. Measurements on samples that represent the structure of a real optical component, such as thin films on a substrate, are therefore much more promising. Such can be studied by EUV reflectometry where the reflectance is measured as a function of wavelength and angle of incidence [12–14]. In the x-ray spectral range, reflectometry (XRR) is an established method to determine the thickness of thin films [15–17] and can also be used to determine the optical constants. EUV reflectometry itself is as easy to realize as a transmission mode experiment, but the interpretation of the results is more complicated.

We present here our results of reflection measurements on thin films of the pure elements Mo, Ni, Pt, Ru, Ta, and Te and different compositions of Ni_xAl_x, Pt_xMo, PtTe, Ru_xTa_x, Ru_3Re, Ru_2W, TaBN, and TaTeN in the range of 62 eV to 124 eV around the energy of 91.85 eV/13.5 nm, which is important for EUV lithography [5]. Dispersion and extinction of these materials are determined through model fits that consider the effects of interdiffusion, surface contamination, and roughness, using a transfer matrix approach [18–20]. The procedure itself is similar to spectroscopic ellipsometry in the optical regime using the Müller-matrix approach for data analysis [21–23].

2. EXPERIMENTAL DETAILS

A. EUV Reflectometry

The experiments were conducted in the Physikalisch-Technische Bundesanstalt (PTB) laboratory at the electron storage ring Berliner Elektronenspeicherring-Gesellschaft für Synchrotronstrahlung (BESSY II) at PTB's soft x-ray beamline [24,25], which covers the photon energy range from 50 eV to 1800 eV. The beamline is designed for a beam with small divergence (regularly below 1 mrad) and minimal halo. The monochromator of the beamline provides a spectral resolution below 0.25 eV. To suppress higher orders, different foil filters (C, B, Be, Si, and Al) have been used, depending on the spectral range [25]. The experimental geometry inside the reflectometer is illustrated in Fig. 1(a). A monochromatic beam with the photon energy $h\nu$ impinges on the sample surface at a variable angle of incidence (aoi) θ_i. The elastically scattered wave propagates along the exit angle θ_f, where the specular reflectance ($\theta_f = \theta_i$) from the sample is measured in s-polarization with a GaAsP photodiode. A lubricant-free goniometer inside the vacuum chamber allows for precise rotation and positioning of the samples, aligning the angle of incidence θ_i with an uncertainty of $\pm 0.01°$ with respect to the incoming beam. An example of an EUV reflectance map, obtained on a Ta sample, is given in Fig. 1(b). The excellent signal-to-noise ratio allows us to resolve the data within more than four orders of magnitude.

B. Sample Preparation

Mo, PtMo, Pt_2Mo, Pt, PtTe, Te, Ni, Ni_3Al, NiAl, Ni_2Al_3, Ru, Ru_3Re, Ru_3Ta, Ru_2W, RuTa, $RuTa_3$, and Ta samples were produced on a silicon wafer substrate using DC magnetron sputtering, which resulted in polycrystalline thin films with nominal thicknesses of 20 nm to 50 nm. The base pressure of the sputter systems was about 10^{-7} mbar, with sputtering performed using argon as process gas at working pressures between 10^{-4} mbar and 5×10^{-3} mbar. Alloys were produced through co-depositing the constituents from separate targets, placed on a rotating wafer drum, resulting in sequential deposition of monolayers and instantaneous intermixing. The TaTeN sample was deposited by reactive co-sputtering of Ta and Te targets in a nitrogen/argon mixture atmosphere. Many different powers, flow rates, gas mixtures, and gas pressures were

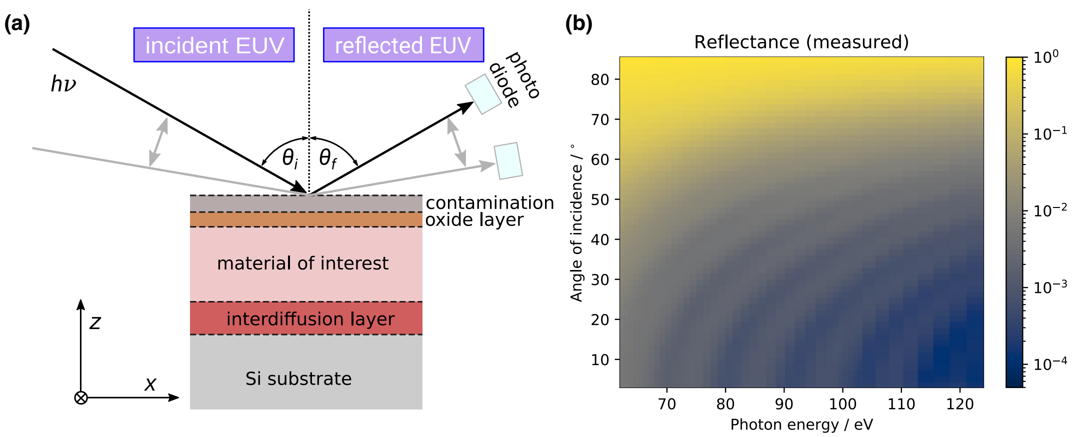

Fig. 1. (a) Sketch of the experimental setup for EUV reflectometry at the soft x-ray beamline of the PTB at the synchrotron radiation facility BESSY II. During a measurement, the angle of incidence θ_i is scanned from grazing to near normal whilst adjusting the position of the photodiode θ_f to detect the specular reflection. The energy is scanned from 62 eV to 124 eV to cover the relevant EUV parts. The setup is operated under vacuum conditions in a lubricant-free environment. (b) Example of an EUV reflectance map, obtained from a Ta thin film on a silicon wafer substrate. The information on optical constants and the sample parameters such as layer thickness and roughness are encoded in the characteristic intensity modulations of the reflectance map.

tried in the process chamber to optimize the compound. The hysteresis effect between the metallic and the poisoned mode was carefully followed by monitoring the cathode voltage. The final composition contained 1:1.45 tantalum and tellurium with below 5% nitrogen content, serving as dopant to reduce oxidation and crystallinity of the sample [3]. The TaBN sample is an industry-representative EUV mask blank, which is commercially available [26]. The composition of the samples was checked by x-ray photoelectron spectroscopy (XPS) or Rutherford backscattering spectrometry (RBS). The typical resulting surface roughness for the samples was classified to be smaller than 0.1 nm (rms) by atomic force microscopy. Diffusion of atoms from the thin film into the substrate leads to an interdiffusion layer of few angstroms thickness at the interface between the deposited material and the substrate. On the surface of the samples, an oxide layer is formed, on top of which an additional contamination layer consisting mainly of water and carbon is found [27]. Depending on the material and the sample's history, an interdiffusion layer and oxide layer built up in varying degrees and therefore had different impacts on the reflectivity of the samples. We find that the thickness of the oxide and the contamination layer varies between almost 0 and 2 nm.

3. THEORETICAL BACKGROUND

EUV reflectometry yields the reflection coefficient R of a sample as a function of the angle of incidence and the photon energy. In the case of a thin film on a substrate, the free parameters are the layer thicknesses h_j, the optical constants of the materials (δ_j, β_j), and the roughness parameters of the interfaces σ_j. Fresnel's equations allow us to calculate reflectivity and transmission at each interface depending on the optical constants, the angle of incidence, and the polarization. Multiple reflections and subsequent passes through the sample lead to interference that determines the total reflectivity of the sample.

A. Matrix Method

The optical properties of thin film samples under monochromatic illumination can be calculated using a transfer matrix approach [12,18,20]. An electromagnetic, monochromatic plane wave can be described by its amplitude A and the k vector. Following Vignaud and Gibaud [20], we use a notation of upwards (+) and downwards (−) traveling waves in the z direction:

$$u^{\pm}(z) = A_j^{\pm} \exp(\pm i k_{z,j} z), \tag{1}$$

which fully describe the state of the system in every layer j (cf. Fig. 1) at the vertical position z. The wave in vacuum, outside the full stack of layers, is given by the following equation:

$$\begin{bmatrix} u^{+}(z_{vac.}) \\ u^{-}(z_{vac.}) \end{bmatrix} = \mathbf{M} \cdot \begin{bmatrix} u^{+}(z_{\text{substrate}}) \\ u^{-}(z_{\text{substrate}}) \end{bmatrix}, \tag{2}$$

which contains the 2 × 2 transfer matrix $\mathbf{M}$, defined as a product of reflection ($\mathbf{R}_{j/k}$) and transmission ($\mathbf{T}_j$) matrices [20]. For a thin film of a specific material (*mat.*) on a substrate, including a contamination layer (*cont.*), an oxide layer (*ox.*), and an interdiffusion layer (*diff.*), this transfer matrix reads

$$\mathbf{M} = \mathbf{R}_{vac./cont.} \cdot \mathbf{T}_{cont.} \cdot \mathbf{R}_{cont./ox.} \cdot \mathbf{T}_{ox.} \cdot \mathbf{R}_{ox./mat.} \cdot \mathbf{T}_{mat.} \cdot \mathbf{R}_{mat./diff.} \cdot \mathbf{T}_{diff.} \cdot \mathbf{R}_{diff./subs.} \tag{3}$$

Further layers can be incorporated by additional transmission and reflection terms. A transmission matrix $\mathbf{T}$ has diagonal form, accounting for absorption and accumulated spectral phase inside the material:

$$\mathbf{T}_j = \begin{bmatrix} \exp(i k_{z,j} h_j) & 0 \\ 0 & \exp(-i k_{z,j} h_j) \end{bmatrix}, \tag{4}$$

with h_j being the thickness of the respective layer. The reflection matrix is calculated from the Fresnel coefficients of the individual interfaces:

$$\mathbf{R}_{j/k} = \begin{bmatrix} p_{j/j-1} & m_{j/j-1} \\ m_{j/j-1} & p_{j/j-1} \end{bmatrix}, \tag{5}$$

with the following coefficients:

$$p_{j/j-1} = \frac{k_{z,j} + k_{z,j-1}}{2k_{z,j}} \cdot \exp\left(-\frac{1}{2}(k_{z,j} + k_{z,j-1})^2 \cdot s_{j/j-1}^2\right),$$

$$m_{j/j-1} = \frac{k_{z,j} - k_{z,j-1}}{2k_{z,j}} \cdot \exp\left(-\frac{1}{2}(k_{z,j} - k_{z,j-1})^2 \cdot s_{j/j-1}^2\right).$$

Imperfections at the interfaces reduce the specular signal. This effect is included here by the exponential term, introducing the interfacial roughness parameter $s_{j/j-1}$ between material j and $(j-1)$ [19]. The optical constants of the materials themselves are encoded in the z component of the wave vectors inside the materials via the refractive index $\tilde{n}_j$ of layer j: $k_{z,j} = \tilde{n}_j \cdot k_{z,vac}$.

To this end, the reflection coefficient R is the ratio of the incoming and outgoing intensity in vacuum $R = \frac{I_{\text{out}}}{I_{\text{in}}}$, calculated from the upwards and downwards traveling plane wave solutions of Eq. (2). After a sufficient distance, the absorption of a bulk substrate would always cancel out all downwards traveling waves $u^{-}(z_{\text{substrate}})$, so upwards traveling waves within the substrate $u^{+}(z_{\text{substrate}})$ do not exist either. Therefore, the reflectivity calculates from only two entries of M_{ij}:

$$R = \frac{I_{\text{out}}}{I_{\text{in}}} = \left|\frac{u^{+}(z_{vac.})}{u^{-}(z_{vac.})}\right|^2 = \left|\frac{M_{12}}{M_{22}}\right|^2. \tag{6}$$

This relationship can be used to calculate the reflectivity of a layered system as a function of photon energy $h\nu$ and angle of incidence θ with the material properties and layer thicknesses as parameters.

B. Optimization Problem

A typical EUV reflectance data set consists of around 45 angles of incidence between near normal and close to 90° at every given photon energy. In a stack of four layers (interdiffusion layer, material of interest, oxide layer, contamination layer) on a substrate (cf. Fig. 1), and assuming that the substrate's optical constants are known, there are 4 × 2 optical constants, five roughness parameters, and four thickness parameters. In the chosen model, the roughness parameters are independent of the wavelength; therefore there are eight unique parameters ($4 \times \delta$ and $4 \times \beta$) at each photon energy, and further nine parameters ($5 \times s$, $4 \times h$) for the global data set across the entire spectrum. Note that the optical constants of all layers are subject to a free-floating fit without further assumptions on them. At 80 measured photon energies, this means that 649 parameters must be determined on a basis of 3600 data points. The optimization problem is defined as follows:

$$\min_{p(\ldots)} \left[\sum_{\nu,\theta} \frac{|R_{calc.}(\nu, \theta) - R_{meas.}(\nu, \theta)|^2}{\sigma_{\nu,\theta}^2} \right], \quad (7)$$

where the calculated values $R_{calc.}$ follow Eq. (6) and the parameters are $p = \{\delta_{j,\nu}; \beta_{j,\nu}; s_j; h_j\}$. The values for the measurement uncertainties $\sigma_{\nu,\theta}$ for all angles and energies were determined from the experimental circumstances [24]. Although the optimization problem in formula (7) could be solved directly, it is more efficient to break it down into two smaller optimization problems. For a fixed set of layer thicknesses and interfacial roughnesses $\{h_j; s_j\}$ as "outer" parameters, the optical constants $\{\delta_{j,\nu}, \beta_{j,\nu}\}$ as "inner" parameters of the optimization problem can be determined individually

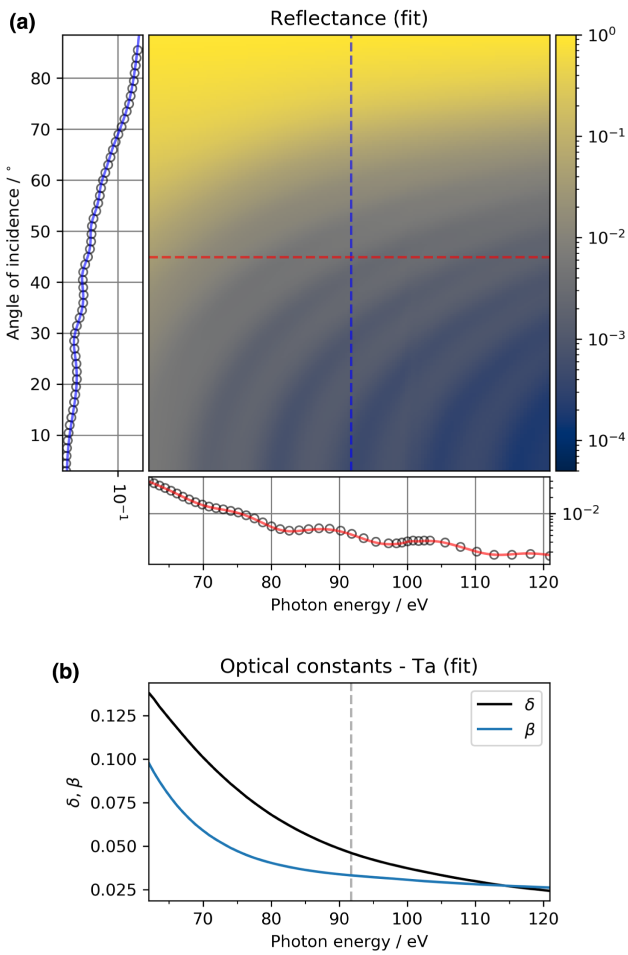

Fig. 2. (a) Simulated EUV reflectance map of the measurement in Fig. 1(b) of a Ta film on silicon. The dashed cross sections beside and below the main panel provide direct comparison with the measured data (circles). (b) Fitted optical constants of the Ta film over the measured spectral range.

for all photon energies using a Levenberg–Marquandt algorithm [28]. Thus, we run a global optimization algorithm [29] to determine the nine 'outer' parameters and minimize the optical constants independently for every measured energy. In this method, the layer's thicknesses are not determined by external methods, but subject to the model fit. Starting values for the optimizer are chosen from prior knowledge of the sample fabrication for s and h, while tabulated data are used for the optical constants [10]. The fitted values for the layer's thicknesses were in general agreement to the design values from the sample preparation process. On a modern desktop computer, this can be solved within reasonable calculation time, using state-of-the-art optimization toolboxes [28–30]. An example of reconstructed reflectance data is given in Fig. 2, underlining that this model is accurately able to describe the experimental data.

4. RESULTS AND DISCUSSION

Table 1 summarizes the optical constants of all measured thin film samples at 91.85 eV/13.5 nm, Fig. 3 presents plots of the data over the full measured spectral range, and the full, spectrally resolved data of all materials measured are reported in Appendix A. Figure 4 compares our results to the existing literature. Next to the optical constants δ and β, Table 1 includes the fitted film thicknesses and material's densities for reference, as well as the chromatic dispersion. In the x-ray region, the refractive index of materials scales linearly with its density, and for high energies far from resonances, the refractive index can be calculated through tabulated atomic scattering factors. We used this to fit the density of our samples by comparing the retrieved optical constants at the highest available photon energy of 124 eV (10 nm) to the Center for X-Ray Optics (CXRO) database [10]. This works well for ruthenium, tantalum, platinum, molybdenum, and tellurium, but in the case of nickel and its alloys, we still find discrepancies to the theoretical data at 124 eV. Since the overall shape of CXRO data agrees well with our data sets, which is shown in Fig. 3, it was used for the approximate determination of the density. We find moderate differences in the density to tabulated data, 15% at maximum. The retrieved density is smaller than the tabulated one, which is not surprising, since the morphology of nanometer scaled thin films is more porous than bulk material. The only exception to this rule is nickel, where we determine a higher density than for bulk, which can be explained through the differences between the reference data and our own measurements [cf. Fig. 3(b) and the resulting poor density fit].

Even in the case in which the main interest lies on the values at a specific photon energy, such as 91.85 eV/13.5 nm, the spectrally resolved measurement and fit are beneficial for the determination of the global sample parameters, such as the layer thicknesses and roughness values. For a single photon energy, the approach used here to model roughness through an interfacial roughness parameter $s_{j/j-1}$ within the Fresnel coefficients [19] does not allow us to discriminate the effect of roughness from interdiffusion between layers. This becomes possible only by including a specific interdiffusion layer in the model (cf. Fig. 1) and measuring what is spectrally resolved. A measurement at the target energy only would result in a less

Table 1. Central Results of the Global Reflectance Fits for Various Thin Layers at 13.5 nm/91.85 eV

	Film Properties		*Refractive Index*		*Chromatic Dispersion*	
Material	**Thickness (nm)**	**Density ($g \cdot cm^{-3}$)[a]**	**δ**	**β**	**$\frac{d\delta}{d\lambda}$ (nm^{-1})**	**$\frac{d\beta}{d\lambda}$ (nm^{-1})**
Mo	27.3	9.5	0.0728	0.0066	−0.015	0.002
PtMo	30.0	15.7	0.0922	0.0344	−0.015	0.012
Pt_2Mo	29.4	17.5	0.0976	0.0416	−0.014	0.015
Pt	34.3	21.1	0.1082	0.0587	−0.012	0.024
PtTe	23.4	11.5	0.0612	0.0751	0.007	0.016
Te	30.7	6.0	0.0352	0.0741	0.012	0.011
Ni	22.3	(10.0)	0.0500	0.0778	−0.002	0.012
Ni_3Al	21.8	(7.1)	0.0225	0.0656	0.002	0.003
NiAl	20.9	(5.8)	0.0110	0.0603	0.005	−0.002
Ni_2Al_3	23.1	(4.5)	0.0058	0.0492	0.006	−0.001
Ru	47.2	11.7	0.1118	0.0154	−0.026	0.010
Ru_3Re	36.3	13.7	0.1035	0.0196	−0.025	0.009
Ru_3Ta	49.1	13.0	0.0940	0.0203	−0.022	0.008
Ru_2W	20.6	14.2	0.0941	0.0201	−0.022	0.008
RuTa	45.5	13.4	0.0747	0.0249	−0.017	0.005
$RuTa_3$	46.9	13.4	0.0593	0.0295	−0.012	0.004
Ta	46.2	14.6	0.0463	0.0335	−0.009	0.002
TaBN	58.7	–	0.0495	0.0318	−0.009	0.003
TaTeN	37.7	6.6	0.0364	0.0438	0.003	0.006

[a]The density is a best-fit value in comparison with the CXRO database [10] at the shortest available wavelength of 10 nm.

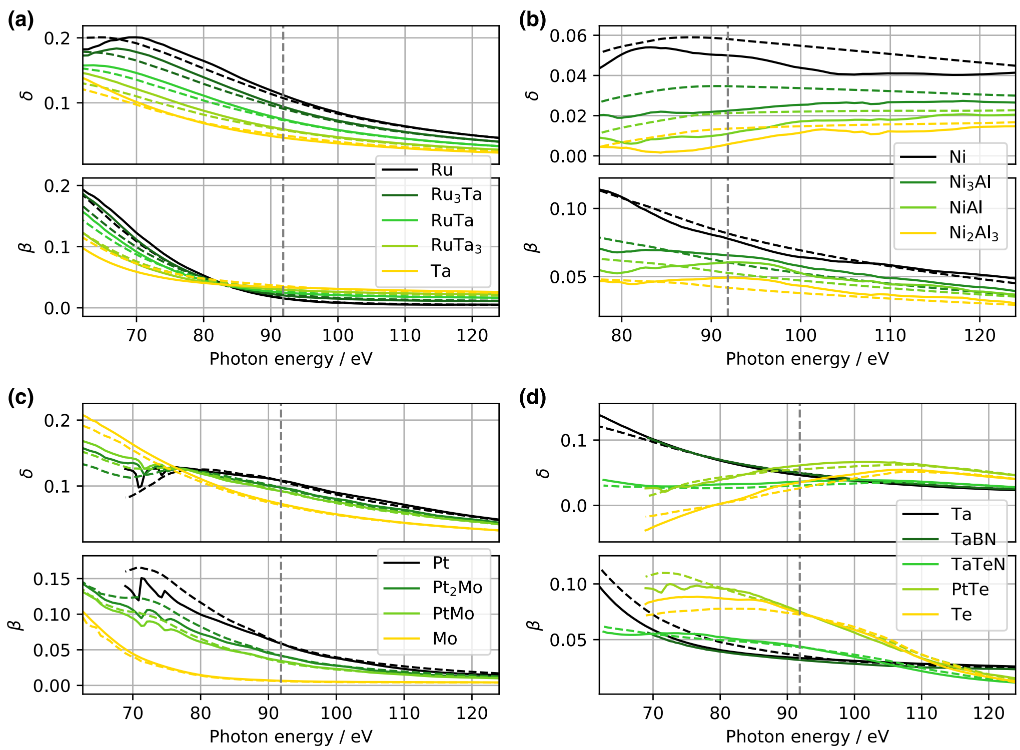

Fig. 3. Spectrally resolved optical constants for different groups of materials (solid lines) and comparison to predictions [10] (dashed lines) with fitted density values (cf. Table 1). Dashed vertical lines indicate 91.85 eV/13.5 nm. (a) Optical constants of ruthenium, tantalum, and their alloys. (b) Optical constants of nickel and nickel aluminum alloys. (c) Optical constants of platinum, molybdenum, and its alloys. Clearly visible are the absorption lines of platinum *N6* at 74.5 eV and *N7* at 71.2 eV. (d) Optical constants of tantalum, tellurium, and various compound materials.

accurate determination of the optical constants because the problem could be over-determined.

Of the pure metals studied here, ruthenium has the largest refractive power, while nickel shows the highest extinction. Platinum comes close to ruthenium, but at a much higher extinction coefficient. The pure metal films mark the extrema in the two-dimensional space of (δ, β), and all the alloys fall in between, as presented in Fig. 5. The numbers for alloyed

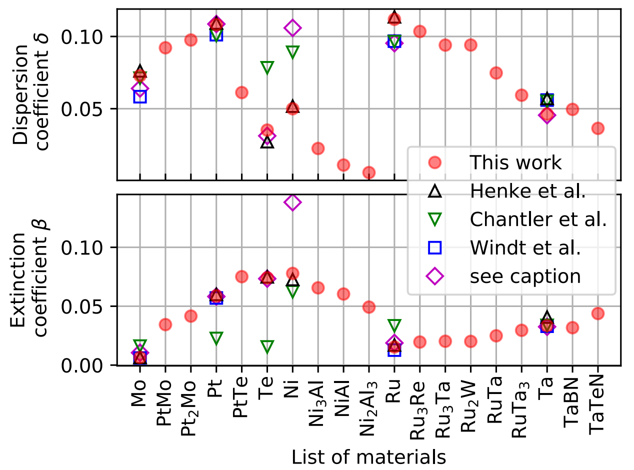

Fig. 4. Comparison of the here presented optical constants at 91.85 eV photon energy/13.5 nm wavelength (red dots) to data from previous studies. From atomic scattering factors: black triangles [10], green triangles [39,40]; from reflectance measurements: blue rectangles [32]. From various other studies: magenta diamonds, Mo [33], Ni [34], Pt [35], Ru [36], Ta [37], and Te [38].

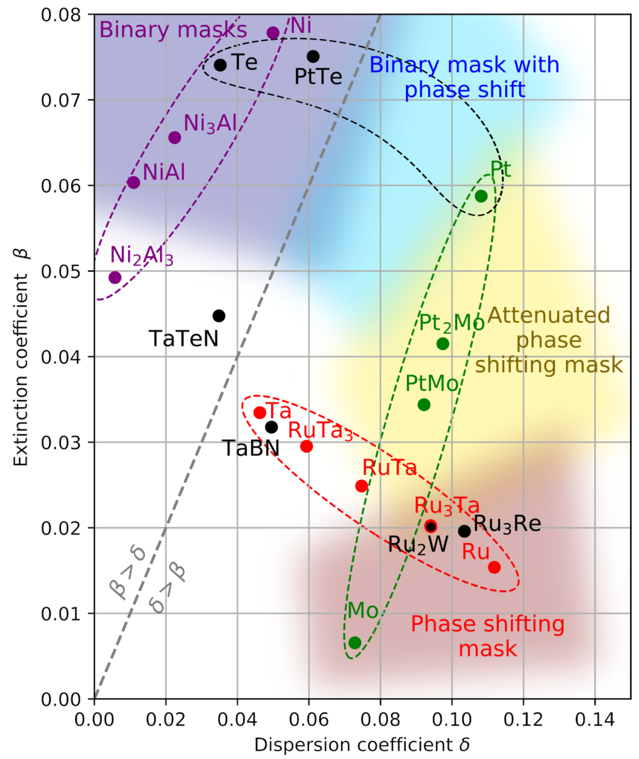

Fig. 5. Optical constants for thin metal films and their alloys at 91.85 eV/13.5 nm, all obtained within this study. Binary alloys are grouped as a guide to the eye. Shaded areas depict regions of interest for different mask-type applications.

metal films suggest that the optical constants of these films can be understood mostly as a weighted sum of their constituents. We find that this is true for alloys of ruthenium and tantalum, molybdenum, and platinum, and chiefly for nickel and aluminum. Although not surprising, these are the first measurements to demonstrate this correlation on the grounds of actual experiments. An interesting exception from this trend is platinum telluride (PtTe), an alloy of the metal platinum and the metalloid tellurium, whose extinction coefficient is larger than that of pure platinum or pure tellurium. The reason lies in the crystal structure of the materials: platinum telluride's orthorhombic crystal structure results in a lower partial specific volume of tellurium than in the trigonal crystal structure of tellurium's pure form [31]. The resulting, higher specific partial mass density of tellurium in platinum telluride is the reason for the large extinction coefficient of the material. We also note that the optical constants of Ru_2W and Ru_3Ta are almost identical, which is because the neighboring elements tungsten and tantalum have very similar densities and therefore a very similar effect on the optical constants of the alloy with ruthenium.

When comparing our data at 91.85 eV to the existing literature of direct measurements of the optical constants [32–38], we find the differences in values, which are summarized in Fig. 4 alongside those calculated from atomic scattering factors [10,39,40]. Of those references, the data of Windt *et al.* on Mo, Pt, Ru, and Ta [32], as well as the data of Rodríguez-de Marcos *et al.* on Te [38] and Hosoya *et al.* on Ta [37], were obtained from reflection-type measurements and are therefore very comparable to ours with respect to methodology and outcome. An exception is the value of Diel *et al.* on Ni [34], which is far from our value and the one from CXRO [10]. Pauly *et al.* used reflection electron energy loss spectroscopy on Mo to determine the dielectric constants [33] and determined a value that is also very close to our value. The data set of Soufli *et al.* on Pt [35], using transmission-type measurements on thin, freestanding films, agrees remarkably well with our data. Differences are smaller than 0.5% over the entire spectral range, including the visible absorption edges *N*6 and *N*7 (not shown).

CXRO data [10] and the data of Chantler [39,40] are based on atomic scattering factors, so the density of the materials is needed as an input to retrieve the optical constants from these databases. For the comparison at 91.85 eV in Fig. 4, we used the tabulated bulk densities instead of the fitted density values of Table 1. The dashed lines in Fig. 3 show that we find good agreement of the CXRO data with our values for many materials over the studied spectral range, if the density is adjusted to the fitted values of Table 1. However, Fig. 4 shows that the values, based on the non-adjusted, tabulated bulk densities, differ at 91.85 eV. Values of the alloys can only be retrieved from the current databases if their density is known. In some spectral regions, such as 70 eV ... 75 eV for platinum, the spectral shape of the optical constants contains additional information about the absorption edges of the materials; see Fig. 3(c). When working near absorption edges, special care needs to be taken, because spectral shifts and polarization effects can occur [41].

5. APPLICATION IN EUV LITHOGRAPHY

The currently most relevant application of the here investigated materials at 13.5 nm wavelength is EUV lithography, namely for reflective photomasks and mirrors. Their development drives the miniaturization of semiconductor technology by enhancing the resolution of the lithography process and thereby reducing the feature sizes on future computer chips. Since the performance of current EUV lithography masks is the result of a rigorous understanding of the image formation process, a key element is the precise knowledge of the refractive index of the materials in use [8,9]. These photomasks are being used today under a chief-ray-angle-at-object (CRAO) of 6°, which corresponds to an angle of incidence range of ≈ 2° … 10° [42]. They consist of a highly reflective multilayer substrate of alternating layers of silicon and molybdenum and an absorber layer on top [43–45]. Compound materials such as TaBN, Ni_3Al [1], RuTa [4], PtMo, or TaTeN [2,3] are currently at the focus of interest for novel absorber materials. Photomasks create a pattern at the wafer based on different physical principles: if most parts of the incoming radiation are absorbed, it is called a 'binary mask'. When phase shifting and successive destructive interference of the reflected radiation play a major role, it is called a 'phase shifting mask' [8]. Figure 5 presents the data of Table 1 as an aerial map to visualize the location of the different materials. In current designs, both effects are being balanced to achieve the best resolution, leading to combinations such as 'binary masks with phase shift' and 'attenuated phase shifting masks'. The areas of interest for such mask materials are marked in the presentation of the optical constants in Fig. 5 through shaded regions. For a binary mask, a high value of the extinction coefficient β is required, while for a hard phase shifting mask, a high value of the dispersion coefficient δ is required, which roughly divides the range of available materials along the line of $\delta = \beta$. Currently, materials with a high dispersion coefficient δ yield the best performance, which means that their real part n of the refractive index is substantially smaller than 1; hence these materials are called low-n [9]. Depending on the precise requirements, different materials or material combinations can be chosen. We find that it is possible to tune the material's properties of a thin film by variation of the alloy's constituents to some extent and position it in between the extreme points, marked by the pure metals. A good example is the system of ruthenium and tantalum, who provide great adjustability of predominantly the dispersion. Platinum and molybdenum, on the other hand, have very similar dispersion values but greatly different extinction coefficients, which allows alloys of the two to be used as an attenuation-adjustable phase shifting material. Nickel–aluminum alloys lie purely within the region of binary masks, but they do not form a completely straight line. This can be understood from the complex shape of the dispersion and extinction curves in Fig. 3(b), which show that both materials contribute greatly to the spectral distribution of their alloys. For platinum, tellurium, and platinum telluride, the case is slightly different, because their crystal structures are all different [31], which means that the density does not follow a straight line on the (δ, β) plane. Apart from their optical properties at 13.5 nm, for non-monochromatic applications the spectral shape is also relevant. The full, spectrally resolved data of all materials measured are reported in Appendix A and in Fig. 3, whereas the chromatic dispersion $\frac{d\tilde{n}}{d\lambda}$ at 13.5 nm wavelength is given in Table 1 as a first order approximation for moderately broadband applications. For the application in EUV lithography masks, other aspects than the optical properties of the materials are equally important for success. Central properties are the ability to deposit and etch the materials, and their stability and resistance against oxidation [8].

6. SUMMARY

We presented optical constants of various pure materials, alloys, and compound materials, measured on thin films in the EUV spectral region. Our results help to give a deeper understanding of the optical properties of materials that are relevant for EUV lithography applications, especially alloys such as Ru_xTa_x and compound materials such as TaTeN. The determination of optical constants was accomplished through a model fit of reflection data over a systematically varying angle of incidence and the photon energy. Using the matrix transfer method to model the reflectance data and modern global optimization schemes, this approach proved to work stably and reliably for a broad set of sample materials. Our results extend the existing literature around the photon energy of 91.85 eV for a variety of materials.

APPENDIX A: DATA TABLES

Complete list of the retrieved optical constants (δ, β) from thin film samples. Wavelengths λ represent the order of measurements; photon energies $h\nu$ are given for reference.

A. Mo

λ/nm	$h\nu$/eV	δ	β
10.00	124.00	0.0326	0.0042
10.20	121.57	0.0342	0.0043
10.40	119.23	0.0360	0.0044
10.60	116.98	0.0377	0.0044
10.80	114.81	0.0395	0.0044
11.00	112.73	0.0415	0.0045
11.20	110.71	0.0435	0.0046
11.40	108.77	0.0455	0.0047
11.60	106.90	0.0476	0.0048
11.80	105.08	0.0499	0.0048
12.00	103.33	0.0522	0.0048
12.20	101.64	0.0546	0.0050
12.40	100.00	0.0571	0.0052
12.60	98.41	0.0597	0.0053
12.80	96.88	0.0625	0.0055
13.00	95.38	0.0653	0.0057
13.20	93.94	0.0682	0.0060
13.40	92.54	0.0713	0.0064
13.60	91.18	0.0744	0.0067
13.80	89.86	0.0776	0.0072
14.00	88.57	0.0809	0.0078
14.20	87.32	0.0844	0.0082
14.40	86.11	0.0879	0.0089
14.60	84.93	0.0917	0.0095
14.80	83.78	0.0957	0.0103
15.00	82.67	0.0998	0.0113
15.20	81.58	0.1041	0.0124
15.40	80.52	0.1085	0.0138
15.60	79.49	0.1130	0.0154
15.80	78.48	0.1175	0.0172
16.00	77.50	0.1221	0.0193
16.20	76.54	0.1267	0.0216
16.40	75.61	0.1313	0.0240

(Table continued)

λ/nm	hν/eV	δ	β
16.60	74.70	0.1359	0.0265
16.80	73.81	0.1406	0.0292
17.00	72.94	0.1454	0.0321
17.20	72.09	0.1503	0.0351
17.40	71.26	0.1551	0.0383
17.60	70.45	0.1602	0.0422
17.80	69.66	0.1653	0.0462
18.00	68.89	0.1703	0.0510
18.20	68.13	0.1752	0.0560
18.40	67.39	0.1800	0.0616
18.60	66.67	0.1843	0.0672
18.80	65.96	0.1885	0.0731
19.00	65.26	0.1925	0.0792
19.20	64.58	0.1976	0.0853
19.40	63.92	0.2000	0.0912
19.60	63.27	0.2044	0.0977
19.80	62.63	0.2076	0.1037

B. PtMo

λ/nm	hν/eV	δ	β
10.00	124.00	0.0420	0.0100
10.20	121.57	0.0450	0.0106
10.50	118.10	0.0482	0.0113
10.80	114.81	0.0516	0.0122
11.00	112.73	0.0551	0.0134
11.20	110.71	0.0588	0.0148
11.50	107.83	0.0624	0.0164
11.80	105.08	0.0659	0.0181
12.00	103.33	0.0694	0.0199
12.20	101.64	0.0729	0.0220
12.50	99.20	0.0765	0.0238
12.80	96.88	0.0804	0.0259
13.00	95.38	0.0843	0.0283
13.20	93.94	0.0884	0.0312
13.50	91.85	0.0922	0.0344
13.80	89.86	0.0956	0.0378
14.00	88.57	0.0988	0.0410
14.20	87.32	0.1017	0.0442
14.50	85.52	0.1048	0.0470
14.80	83.78	0.1082	0.0504
15.00	82.67	0.1116	0.0536
15.20	81.58	0.1151	0.0570
15.50	80.00	0.1188	0.0610
15.60	79.49	0.1202	0.0625
15.70	78.98	0.1218	0.0644
15.80	78.48	0.1233	0.0665
15.90	77.99	0.1248	0.0689
16.00	77.50	0.1258	0.0715
16.10	77.02	0.1263	0.0741
16.20	76.54	0.1264	0.0762
16.30	76.07	0.1263	0.0778
16.40	75.61	0.1258	0.0788
16.50	75.15	0.1252	0.0776
16.60	74.70	0.1291	0.0775
16.70	74.25	0.1323	0.0817
16.80	73.81	0.1328	0.0856
16.90	73.37	0.1323	0.0879
17.00	72.94	0.1313	0.0892

(Table continued)

λ/nm	hν/eV	δ	β
17.10	72.51	0.1299	0.0900
17.20	72.09	0.1274	0.0897
17.30	71.68	0.1260	0.0840
17.40	71.26	0.1335	0.0834
17.50	70.86	0.1384	0.0877
17.60	70.45	0.1407	0.0914
17.70	70.06	0.1416	0.0942
17.80	69.66	0.1425	0.0959
17.90	69.27	0.1431	0.0982
18.00	68.89	0.1435	0.0996
18.20	68.13	0.1454	0.1026
18.50	67.03	0.1492	0.1052
18.80	65.96	0.1536	0.1097
19.00	65.26	0.1578	0.1142
19.20	64.58	0.1614	0.1205
19.50	63.59	0.1650	0.1260
19.80	62.63	0.1682	0.1313

C. Pt_2Mo

λ/nm	hν/eV	δ	β
10.00	124.00	0.0443	0.0115
10.20	121.57	0.0477	0.0122
10.50	118.10	0.0513	0.0131
10.80	114.81	0.0550	0.0142
11.00	112.73	0.0589	0.0156
11.20	110.71	0.0628	0.0173
11.50	107.83	0.0667	0.0192
11.80	105.08	0.0705	0.0214
12.00	103.33	0.0743	0.0237
12.20	101.64	0.0780	0.0261
12.50	99.20	0.0816	0.0285
12.80	96.88	0.0858	0.0310
13.00	95.38	0.0898	0.0340
13.20	93.94	0.0940	0.0375
13.50	91.85	0.0976	0.0416
13.80	89.86	0.1007	0.0457
14.00	88.57	0.1036	0.0496
14.20	87.32	0.1061	0.0532
14.50	85.52	0.1088	0.0567
14.80	83.78	0.1116	0.0605
15.00	82.67	0.1145	0.0644
15.20	81.58	0.1176	0.0682
15.50	80.00	0.1206	0.0727
15.60	79.49	0.1219	0.0746
15.70	78.98	0.1230	0.0765
15.80	78.48	0.1243	0.0786
15.90	77.99	0.1254	0.0810
16.00	77.50	0.1264	0.0838
16.10	77.02	0.1267	0.0867
16.20	76.54	0.1262	0.0894
16.30	76.07	0.1254	0.0918
16.40	75.61	0.1240	0.0933
16.50	75.15	0.1222	0.0926
16.60	74.70	0.1251	0.0904
16.70	74.25	0.1293	0.0940
16.80	73.81	0.1302	0.0982
16.90	73.37	0.1292	0.1022
17.00	72.94	0.1270	0.1045

(Table continued)

λ/nm	$h\nu$/eV	δ	β
17.10	72.51	0.1243	0.1058
17.20	72.09	0.1204	0.1058
17.30	71.68	0.1170	0.1001
17.40	71.26	0.1246	0.0944
17.50	70.86	0.1313	0.0983
17.60	70.45	0.1339	0.1024
17.70	70.06	0.1347	0.1058
17.80	69.66	0.1348	0.1081
17.90	69.27	0.1344	0.1104
18.00	68.89	0.1350	0.1118
18.20	68.13	0.1359	0.1143
18.50	67.03	0.1399	0.1162
18.80	65.96	0.1428	0.1201
19.00	65.26	0.1475	0.1245
19.20	64.58	0.1509	0.1301
19.50	63.59	0.1537	0.1365
19.80	62.63	0.1574	0.1429

D. Pt

λ/nm	$h\nu$/eV	δ	β
10.00	124.00	0.0490	0.0144
10.10	122.77	0.0506	0.0148
10.20	121.57	0.0522	0.0152
10.30	120.39	0.0538	0.0156
10.40	119.23	0.0555	0.0161
10.50	118.10	0.0573	0.0166
10.60	116.98	0.0591	0.0172
10.70	115.89	0.0609	0.0178
10.80	114.81	0.0628	0.0186
10.90	113.76	0.0647	0.0194
11.00	112.73	0.0666	0.0204
11.10	111.71	0.0684	0.0214
11.20	110.71	0.0703	0.0224
11.30	109.73	0.0721	0.0235
11.40	108.77	0.0739	0.0247
11.50	107.83	0.0757	0.0259
11.60	106.90	0.0775	0.0272
11.70	105.98	0.0792	0.0285
11.80	105.08	0.0809	0.0300
11.90	104.20	0.0824	0.0315
12.00	103.33	0.0838	0.0329
12.10	102.48	0.0853	0.0341
12.20	101.64	0.0869	0.0355
12.30	100.81	0.0883	0.0370
12.40	100.00	0.0897	0.0382
12.50	99.20	0.0914	0.0394
12.60	98.41	0.0932	0.0406
12.70	97.64	0.0952	0.0422
12.80	96.88	0.0970	0.0439
12.90	96.12	0.0988	0.0457
13.00	95.38	0.1005	0.0476
13.10	94.66	0.1022	0.0494
13.20	93.94	0.1041	0.0515
13.30	93.23	0.1058	0.0539
13.40	92.54	0.1071	0.0564
13.50	91.85	0.1082	0.0587
13.60	91.18	0.1092	0.0608
13.70	90.51	0.1105	0.0631

(Table continued)

λ/nm	$h\nu$/eV	δ	β
13.80	89.86	0.1116	0.0654
13.90	89.21	0.1125	0.0679
14.00	88.57	0.1131	0.0703
14.10	87.94	0.1136	0.0723
14.20	87.32	0.1142	0.0741
14.30	86.71	0.1150	0.0760
14.40	86.11	0.1159	0.0781
14.50	85.52	0.1167	0.0801
14.60	84.93	0.1173	0.0822
14.70	84.35	0.1180	0.0842
14.80	83.78	0.1187	0.0862
14.90	83.22	0.1195	0.0883
15.00	82.67	0.1200	0.0904
15.10	82.12	0.1204	0.0924
15.20	81.58	0.1210	0.0942
15.30	81.05	0.1217	0.0959
15.40	80.52	0.1226	0.0976
15.50	80.00	0.1238	0.0996
15.60	79.49	0.1248	0.1019
15.70	78.98	0.1256	0.1043
15.80	78.48	0.1262	0.1069
15.90	77.99	0.1269	0.1094
16.00	77.50	0.1270	0.1120
16.10	77.02	0.1276	0.1142
16.20	76.54	0.1284	0.1170
16.30	76.07	0.1286	0.1206
16.40	75.61	0.1283	0.1245
16.50	75.15	0.1267	0.1288
16.60	74.70	0.1209	0.1328
16.70	74.25	0.1162	0.1236
16.80	73.81	0.1252	0.1255
16.90	73.37	0.1265	0.1306
17.00	72.94	0.1262	0.1349
17.10	72.51	0.1250	0.1392
17.20	72.09	0.1225	0.1440
17.30	71.68	0.1164	0.1498
17.40	71.26	0.0999	0.1506
17.50	70.86	0.0977	0.1194
17.60	70.45	0.1179	0.1230
17.70	70.06	0.1226	0.1295
17.80	69.66	0.1240	0.1339
17.90	69.27	0.1249	0.1370
18.00	68.89	0.1259	0.1396

E. PtTe

λ/nm	$h\nu$/eV	δ	β
10.00	124.00	0.0461	0.0153
10.10	122.77	0.0473	0.0165
10.20	121.57	0.0487	0.0177
10.30	120.39	0.0501	0.0185
10.40	119.23	0.0515	0.0195
10.50	118.10	0.0529	0.0209
10.60	116.98	0.0540	0.0224
10.70	115.89	0.0555	0.0236
10.80	114.81	0.0572	0.0254
10.90	113.76	0.0578	0.0272
11.00	112.73	0.0592	0.0285
11.10	111.71	0.0603	0.0302
11.20	110.71	0.0613	0.0321

(Table continued)

λ/nm	$h\nu$/eV	δ	β
11.30	109.73	0.0625	0.0339
11.40	108.77	0.0640	0.0361
11.50	107.83	0.0633	0.0398
11.60	106.90	0.0643	0.0401
11.70	105.98	0.0658	0.0425
11.80	105.08	0.0655	0.0444
11.90	104.20	0.0659	0.0467
12.00	103.33	0.0662	0.0486
12.10	102.48	0.0665	0.0504
12.20	101.64	0.0666	0.0524
12.30	100.81	0.0665	0.0543
12.40	100.00	0.0663	0.0563
12.50	99.20	0.0660	0.0582
12.60	98.41	0.0659	0.0600
12.70	97.64	0.0656	0.0617
12.80	96.88	0.0653	0.0635
12.90	96.12	0.0649	0.0651
13.00	95.38	0.0645	0.0668
13.10	94.66	0.0638	0.0685
13.20	93.94	0.0631	0.0704
13.30	93.23	0.0627	0.0718
13.40	92.54	0.0619	0.0736
13.50	91.85	0.0612	0.0751
13.60	91.18	0.0605	0.0767
13.70	90.51	0.0596	0.0784
13.80	89.86	0.0590	0.0797
13.90	89.21	0.0581	0.0813
14.00	88.57	0.0574	0.0827
14.10	87.94	0.0568	0.0838
14.20	87.32	0.0554	0.0854
14.30	86.71	0.0545	0.0866
14.40	86.11	0.0529	0.0883
14.50	85.52	0.0520	0.0895
14.60	84.93	0.0507	0.0905
14.70	84.35	0.0487	0.0919
14.80	83.78	0.0476	0.0925
14.90	83.22	0.0462	0.0932
15.00	82.67	0.0455	0.0935
15.10	82.12	0.0430	0.0949
15.20	81.58	0.0422	0.0949
15.30	81.05	0.0407	0.0956
15.40	80.52	0.0405	0.0955
15.50	80.00	0.0391	0.0959
15.60	79.49	0.0380	0.0965
15.70	78.98	0.0359	0.0970
15.80	78.48	0.0355	0.0970
15.90	77.99	0.0352	0.0968
16.00	77.50	0.0345	0.0974
16.10	77.02	0.0328	0.0979
16.20	76.54	0.0316	0.0985
16.30	76.07	0.0311	0.0979
16.40	75.61	0.0295	0.0975
16.50	75.15	0.0284	0.0959
16.60	74.70	0.0285	0.0950
16.70	74.25	0.0290	0.0953
16.80	73.81	0.0290	0.0967
17.00	72.94	0.0266	0.0994
17.10	72.51	0.0243	0.0998
17.20	72.09	0.0217	0.0992
17.30	71.68	0.0207	0.0958
17.40	71.26	0.0231	0.0921
17.50	70.86	0.0260	0.0928
17.60	70.45	0.0263	0.0942
17.70	70.06	0.0264	0.0953
17.80	69.66	0.0264	0.0958
17.90	69.27	0.0262	0.0960
18.00	68.89	0.0261	0.0961

(Table continued)

F. Te

λ/nm	$h\nu$/eV	δ	β
10.00	124.00	0.0403	0.0127
10.10	122.77	0.0413	0.0137
10.20	121.57	0.0424	0.0148
10.30	120.39	0.0435	0.0160
10.40	119.23	0.0446	0.0172
10.50	118.10	0.0458	0.0185
10.60	116.98	0.0469	0.0199
10.70	115.89	0.0481	0.0214
10.80	114.81	0.0493	0.0231
10.90	113.76	0.0504	0.0249
11.00	112.73	0.0514	0.0269
11.10	111.71	0.0523	0.0290
11.20	110.71	0.0532	0.0313
11.30	109.73	0.0537	0.0336
11.40	108.77	0.0543	0.0361
11.50	107.83	0.0546	0.0387
11.60	106.90	0.0546	0.0413
11.70	105.98	0.0545	0.0440
11.80	105.08	0.0540	0.0467
11.90	104.20	0.0533	0.0492
12.00	103.33	0.0523	0.0515
12.10	102.48	0.0513	0.0536
12.20	101.64	0.0501	0.0555
12.30	100.81	0.0490	0.0572
12.40	100.00	0.0478	0.0588
12.50	99.20	0.0467	0.0602
12.60	98.41	0.0457	0.0616
12.70	97.64	0.0448	0.0631
12.80	96.88	0.0438	0.0646
12.90	96.12	0.0428	0.0662
13.00	95.38	0.0417	0.0677
13.10	94.66	0.0405	0.0692
13.20	93.94	0.0392	0.0706
13.30	93.23	0.0378	0.0718
13.40	92.54	0.0364	0.0730
13.50	91.85	0.0352	0.0741
13.60	91.18	0.0340	0.0751
13.70	90.51	0.0330	0.0763
13.80	89.86	0.0319	0.0775
13.90	89.21	0.0307	0.0789
14.00	88.57	0.0293	0.0803
14.10	87.94	0.0277	0.0817
14.20	87.32	0.0258	0.0830
14.30	86.71	0.0236	0.0841
14.40	86.11	0.0213	0.0849
14.50	85.52	0.0189	0.0854
14.60	84.93	0.0166	0.0858
14.70	84.35	0.0145	0.0859

(Table continued)

λ/nm	$h\nu$/eV	δ	β
14.80	83.78	0.0125	0.0859
14.90	83.22	0.0107	0.0858
15.00	82.67	0.0091	0.0857
15.10	82.12	0.0076	0.0860
15.20	81.58	0.0062	0.0863
15.30	81.05	0.0050	0.0865
15.40	80.52	0.0037	0.0868
15.50	80.00	0.0025	0.0872
15.60	79.49	0.0012	0.0872
15.70	78.98	−0.0001	0.0877
15.80	78.48	−0.0016	0.0880
15.90	77.99	−0.0030	0.0880
16.00	77.50	−0.0046	0.0881
16.10	77.02	−0.0063	0.0883
16.20	76.54	−0.0079	0.0884
16.30	76.07	−0.0095	0.0883
16.40	75.61	−0.0111	0.0882
16.50	75.15	−0.0127	0.0882
16.60	74.70	−0.0144	0.0883
16.70	74.25	−0.0159	0.0880
16.80	73.81	−0.0176	0.0881
16.90	73.37	−0.0194	0.0879
17.00	72.94	−0.0211	0.0876
17.10	72.51	−0.0228	0.0873
17.20	72.09	−0.0245	0.0868
17.30	71.68	−0.0262	0.0865
17.40	71.26	−0.0278	0.0860
17.50	70.86	−0.0295	0.0857
17.60	70.45	−0.0312	0.0851
17.70	70.06	−0.0330	0.0845
17.80	69.66	−0.0348	0.0838
17.90	69.27	−0.0369	0.0833
18.00	68.89	−0.0383	0.0819

G. Ni

λ/nm	$h\nu$/eV	δ	β
10.00	124.00	0.0414	0.0486
10.10	122.77	0.0411	0.0495
10.20	121.57	0.0409	0.0504
10.30	120.39	0.0406	0.0511
10.40	119.23	0.0404	0.0518
10.50	118.10	0.0403	0.0525
10.60	116.98	0.0403	0.0530
10.70	115.89	0.0404	0.0535
10.80	114.81	0.0407	0.0541
10.90	113.76	0.0409	0.0551
11.00	112.73	0.0410	0.0561
11.10	111.71	0.0410	0.0569
11.20	110.71	0.0410	0.0578
11.30	109.73	0.0411	0.0586
11.40	108.77	0.0409	0.0594
11.50	107.83	0.0408	0.0597
11.60	106.90	0.0408	0.0600
11.70	105.98	0.0405	0.0602
11.80	105.08	0.0406	0.0610
11.90	104.20	0.0407	0.0611
12.00	103.33	0.0412	0.0616
12.10	102.48	0.0420	0.0626
12.20	101.64	0.0427	0.0633
12.30	100.81	0.0433	0.0638
12.40	100.00	0.0438	0.0643
12.50	99.20	0.0443	0.0650
12.60	98.41	0.0452	0.0660
12.70	97.64	0.0460	0.0671
12.80	96.88	0.0468	0.0683
12.90	96.12	0.0476	0.0696
13.00	95.38	0.0482	0.0710
13.10	94.66	0.0488	0.0725
13.20	93.94	0.0492	0.0738
13.30	93.23	0.0495	0.0753
13.40	92.54	0.0498	0.0766
13.50	91.85	0.0500	0.0778
13.60	91.18	0.0502	0.0792
13.70	90.51	0.0503	0.0801
13.80	89.86	0.0504	0.0811
13.90	89.21	0.0507	0.0822
14.00	88.57	0.0511	0.0832
14.10	87.94	0.0512	0.0842
14.20	87.32	0.0519	0.0854
14.30	86.71	0.0523	0.0864
14.40	86.11	0.0529	0.0881
14.50	85.52	0.0533	0.0896
14.60	84.93	0.0536	0.0914
14.70	84.35	0.0536	0.0931
14.80	83.78	0.0539	0.0951
14.90	83.22	0.0540	0.0969
15.00	82.67	0.0540	0.0989
15.10	82.12	0.0536	0.1004
15.20	81.58	0.0531	0.1025
15.30	81.05	0.0525	0.1046
15.40	80.52	0.0516	0.1068
15.50	80.00	0.0505	0.1084
15.60	79.49	0.0492	0.1099
15.70	78.98	0.0477	0.1111
15.80	78.48	0.0463	0.1124
15.90	77.99	0.0448	0.1131
16.00	77.50	0.0435	0.1139

H. Ni_3Al

λ/nm	$h\nu$/eV	δ	β
10.00	124.00	0.0265	0.0394
10.10	122.77	0.0267	0.0405
10.20	121.57	0.0268	0.0415
10.30	120.39	0.0269	0.0421
10.40	119.23	0.0272	0.0426
10.50	118.10	0.0274	0.0433
10.60	116.98	0.0270	0.0441
10.70	115.89	0.0270	0.0449
10.80	114.81	0.0269	0.0458
10.90	113.76	0.0268	0.0467
11.00	112.73	0.0268	0.0475
11.10	111.71	0.0268	0.0480
11.20	110.71	0.0267	0.0487
11.30	109.73	0.0267	0.0489
11.40	108.77	0.0259	0.0496
11.50	107.83	0.0258	0.0509
11.60	106.90	0.0265	0.0518
11.70	105.98	0.0263	0.0521

(Table continued)

λ/nm	$h\nu$/eV	δ	β
11.80	105.08	0.0265	0.0533
11.90	104.20	0.0263	0.0540
12.00	103.33	0.0263	0.0546
12.10	102.48	0.0262	0.0554
12.20	101.64	0.0260	0.0556
12.30	100.81	0.0255	0.0565
12.40	100.00	0.0254	0.0577
12.50	99.20	0.0253	0.0585
12.60	98.41	0.0250	0.0595
12.70	97.64	0.0248	0.0609
12.80	96.88	0.0245	0.0619
12.90	96.12	0.0242	0.0629
13.00	95.38	0.0238	0.0636
13.10	94.66	0.0235	0.0641
13.20	93.94	0.0232	0.0646
13.30	93.23	0.0230	0.0650
13.40	92.54	0.0227	0.0653
13.50	91.85	0.0225	0.0656
13.60	91.18	0.0222	0.0660
13.70	90.51	0.0220	0.0664
13.80	89.86	0.0219	0.0666
13.90	89.21	0.0217	0.0669
14.00	88.57	0.0215	0.0672
14.10	87.94	0.0213	0.0676
14.20	87.32	0.0214	0.0678
14.30	86.71	0.0214	0.0682
14.40	86.11	0.0214	0.0687
14.50	85.52	0.0216	0.0689
14.60	84.93	0.0219	0.0690
14.70	84.35	0.0220	0.0694
14.80	83.78	0.0217	0.0694
14.90	83.22	0.0215	0.0694
15.00	82.67	0.0210	0.0696
15.10	82.12	0.0204	0.0693
15.20	81.58	0.0200	0.0690
15.30	81.05	0.0195	0.0684
15.40	80.52	0.0193	0.0684
15.50	80.00	0.0190	0.0680
15.60	79.49	0.0190	0.0678
15.70	78.98	0.0197	0.0680
15.80	78.48	0.0202	0.0688
15.90	77.99	0.0204	0.0697
16.00	77.50	0.0202	0.0706

I. NiAl

λ/nm	$h\nu$/eV	δ	β
10.00	124.00	0.0205	0.0367
10.10	122.77	0.0203	0.0375
10.20	121.57	0.0202	0.0382
10.30	120.39	0.0202	0.0389
10.40	119.23	0.0205	0.0391
10.50	118.10	0.0207	0.0407
10.60	116.98	0.0205	0.0419
10.70	115.89	0.0204	0.0427
10.80	114.81	0.0199	0.0434
10.90	113.76	0.0193	0.0438
11.00	112.73	0.0187	0.0440
11.10	111.71	0.0183	0.0441
11.20	110.71	0.0181	0.0442
11.30	109.73	0.0180	0.0443
11.40	108.77	0.0183	0.0457
11.50	107.83	0.0178	0.0468
11.60	106.90	0.0180	0.0465
11.70	105.98	0.0180	0.0471
11.80	105.08	0.0177	0.0478
11.90	104.20	0.0176	0.0483
12.00	103.33	0.0176	0.0488
12.10	102.48	0.0176	0.0493
12.20	101.64	0.0176	0.0500
12.30	100.81	0.0173	0.0511
12.40	100.00	0.0171	0.0526
12.50	99.20	0.0167	0.0541
12.60	98.41	0.0162	0.0557
12.70	97.64	0.0155	0.0573
12.80	96.88	0.0147	0.0585
12.90	96.12	0.0140	0.0593
13.00	95.38	0.0135	0.0598
13.10	94.66	0.0131	0.0601
13.20	93.94	0.0127	0.0603
13.30	93.23	0.0122	0.0604
13.40	92.54	0.0116	0.0605
13.50	91.85	0.0110	0.0603
13.60	91.18	0.0105	0.0601
13.70	90.51	0.0101	0.0598
13.80	89.86	0.0098	0.0596
13.90	89.21	0.0096	0.0593
14.00	88.57	0.0094	0.0589
14.10	87.94	0.0094	0.0585
14.20	87.32	0.0095	0.0580
14.30	86.71	0.0096	0.0579
14.40	86.11	0.0095	0.0577
14.50	85.52	0.0092	0.0576
14.60	84.93	0.0088	0.0573
14.70	84.35	0.0085	0.0566
14.80	83.78	0.0083	0.0562
14.90	83.22	0.0082	0.0564
15.00	82.67	0.0077	0.0566
15.10	82.12	0.0068	0.0562
15.20	81.58	0.0062	0.0551
15.30	81.05	0.0061	0.0540
15.40	80.52	0.0062	0.0533
15.50	80.00	0.0068	0.0528
15.60	79.49	0.0072	0.0524
15.70	78.98	0.0080	0.0528
15.80	78.48	0.0084	0.0532
15.90	77.99	0.0088	0.0540
16.00	77.50	0.0091	0.0548

J. Ni_2Al_3

λ/nm	$h\nu$/eV	δ	β
10.00	124.00	0.0147	0.0304
10.10	122.77	0.0147	0.0316
10.20	121.57	0.0145	0.0320
10.30	120.39	0.0145	0.0327
10.40	119.23	0.0143	0.0335
10.50	118.10	0.0137	0.0345
10.60	116.98	0.0131	0.0346
10.70	115.89	0.0129	0.0349

(Table continued)

λ/nm	$h\nu$/eV	δ	β
10.80	114.81	0.0125	0.0351
10.90	113.76	0.0122	0.0351
11.00	112.73	0.0122	0.0354
11.10	111.71	0.0121	0.0357
11.20	110.71	0.0121	0.0361
11.30	109.73	0.0122	0.0369
11.40	108.77	0.0110	0.0371
11.50	107.83	0.0108	0.0366
11.60	106.90	0.0121	0.0372
11.70	105.98	0.0118	0.0377
11.80	105.08	0.0124	0.0385
11.90	104.20	0.0125	0.0393
12.00	103.33	0.0129	0.0401
12.10	102.48	0.0132	0.0409
12.20	101.64	0.0129	0.0416
12.30	100.81	0.0122	0.0428
12.40	100.00	0.0115	0.0433
12.50	99.20	0.0110	0.0437
12.60	98.41	0.0106	0.0446
12.70	97.64	0.0103	0.0460
12.80	96.88	0.0098	0.0468
12.90	96.12	0.0092	0.0476
13.00	95.38	0.0086	0.0480
13.10	94.66	0.0081	0.0484
13.20	93.94	0.0075	0.0487
13.30	93.23	0.0069	0.0490
13.40	92.54	0.0064	0.0493
13.50	91.85	0.0058	0.0492
13.60	91.18	0.0051	0.0492
13.70	90.51	0.0046	0.0489
13.80	89.86	0.0041	0.0486
13.90	89.21	0.0036	0.0484
14.00	88.57	0.0032	0.0481
14.10	87.94	0.0027	0.0479
14.20	87.32	0.0026	0.0478
14.30	86.71	0.0024	0.0478
14.40	86.11	0.0021	0.0476
14.50	85.52	0.0021	0.0474
14.60	84.93	0.0020	0.0470
14.70	84.35	0.0016	0.0468
14.80	83.78	0.0019	0.0464
14.90	83.22	0.0020	0.0462
15.00	82.67	0.0021	0.0457
15.10	82.12	0.0025	0.0451
15.20	81.58	0.0031	0.0446
15.30	81.05	0.0036	0.0445
15.40	80.52	0.0040	0.0449
15.50	80.00	0.0040	0.0457
15.60	79.49	0.0041	0.0461
15.70	78.98	0.0043	0.0459
15.80	78.48	0.0044	0.0462
15.90	77.99	0.0044	0.0467
16.00	77.50	0.0046	0.0467

K. Ru

λ/nm	$h\nu$/eV	δ	β
10.00	124.00	0.0460	0.0052
10.25	120.98	0.0491	0.0053
10.50	118.10	0.0523	0.0052
10.75	115.35	0.0559	0.0050
11.00	112.73	0.0596	0.0052
11.25	110.22	0.0637	0.0053
11.50	107.83	0.0677	0.0056
11.75	105.53	0.0723	0.0062
12.00	103.33	0.0769	0.0069
12.10	102.48	0.0789	0.0072
12.20	101.64	0.0807	0.0077
12.30	100.81	0.0828	0.0084
12.40	100.00	0.0853	0.0084
12.50	99.20	0.0874	0.0084
12.60	98.41	0.0896	0.0089
12.75	97.25	0.0930	0.0095
13.00	95.38	0.0990	0.0111
13.25	93.58	0.1053	0.0130
13.50	91.85	0.1118	0.0154
13.75	90.18	0.1185	0.0181
14.00	88.57	0.1250	0.0213
14.25	87.02	0.1315	0.0250
14.50	85.52	0.1382	0.0294
14.75	84.07	0.1454	0.0346
15.00	82.67	0.1526	0.0404
15.25	81.31	0.1590	0.0464
15.50	80.00	0.1645	0.0528
15.75	78.73	0.1694	0.0592
16.00	77.50	0.1744	0.0655
16.25	76.31	0.1794	0.0725
16.50	75.15	0.1840	0.0804
16.75	74.03	0.1893	0.0886
17.00	72.94	0.1928	0.0974
17.25	71.88	0.1971	0.1066
17.50	70.86	0.2002	0.1150
17.75	69.86	0.2008	0.1237
18.00	68.89	0.2007	0.1337
18.25	67.95	0.1991	0.1433
18.50	67.03	0.1967	0.1521
18.75	66.13	0.1960	0.1607
19.00	65.26	0.1927	0.1676
19.25	64.42	0.1882	0.1760
19.50	63.59	0.1856	0.1825
19.75	62.78	0.1824	0.1870
20.00	62.00	0.1822	0.1934

L. Ru_3Re

λ/nm	$h\nu$/eV	δ	β
10.00	124.00	0.0425	0.0105
10.10	122.77	0.0435	0.0106
10.20	121.57	0.0446	0.0108
10.30	120.39	0.0456	0.0106
10.40	119.23	0.0466	0.0104
10.50	118.10	0.0479	0.0104
10.60	116.98	0.0491	0.0104
10.70	115.89	0.0504	0.0102
10.80	114.81	0.0521	0.0103
10.90	113.76	0.0533	0.0105
11.00	112.73	0.0546	0.0103
11.10	111.71	0.0562	0.0104
11.20	110.71	0.0577	0.0103
11.30	109.73	0.0593	0.0103

(Table continued)

λ/nm	$h\nu$/eV	δ	β
11.40	108.77	0.0615	0.0109
11.50	107.83	0.0627	0.0118
11.60	106.90	0.0637	0.0108
11.70	105.98	0.0661	0.0115
11.80	105.08	0.0671	0.0112
11.90	104.20	0.0692	0.0116
12.00	103.33	0.0709	0.0117
12.10	102.48	0.0727	0.0120
12.20	101.64	0.0746	0.0124
12.30	100.81	0.0766	0.0128
12.40	100.00	0.0787	0.0130
12.50	99.20	0.0807	0.0132
12.60	98.41	0.0827	0.0136
12.70	97.64	0.0848	0.0141
12.80	96.88	0.0870	0.0146
12.90	96.12	0.0893	0.0152
13.00	95.38	0.0915	0.0157
13.10	94.66	0.0938	0.0163
13.20	93.94	0.0962	0.0170
13.30	93.23	0.0986	0.0178
13.40	92.54	0.1010	0.0187
13.50	91.85	0.1035	0.0196
13.60	91.18	0.1060	0.0205
13.70	90.51	0.1085	0.0215
13.80	89.86	0.1110	0.0226
13.90	89.21	0.1135	0.0239
14.00	88.57	0.1161	0.0252
14.10	87.94	0.1187	0.0265
14.20	87.32	0.1213	0.0279
14.30	86.71	0.1239	0.0295
14.40	86.11	0.1265	0.0311
14.50	85.52	0.1291	0.0328
14.60	84.93	0.1317	0.0346
14.70	84.35	0.1342	0.0364
14.80	83.78	0.1367	0.0383
14.90	83.22	0.1392	0.0403
15.00	82.67	0.1416	0.0424
15.10	82.12	0.1440	0.0445
15.20	81.58	0.1464	0.0467
15.30	81.05	0.1488	0.0489
15.40	80.52	0.1511	0.0512
15.50	80.00	0.1535	0.0536
15.60	79.49	0.1558	0.0559
15.70	78.98	0.1582	0.0584
15.80	78.48	0.1605	0.0609
15.90	77.99	0.1627	0.0635
16.00	77.50	0.1651	0.0662
16.10	77.02	0.1673	0.0690
16.20	76.54	0.1695	0.0719
16.30	76.07	0.1716	0.0749
16.40	75.61	0.1737	0.0778
16.50	75.15	0.1757	0.0810
16.60	74.70	0.1777	0.0842
16.70	74.25	0.1795	0.0873
16.80	73.81	0.1812	0.0905
16.90	73.37	0.1828	0.0938
17.00	72.94	0.1843	0.0969
17.10	72.51	0.1857	0.1001
17.20	72.09	0.1871	0.1034
17.30	71.68	0.1884	0.1068
17.40	71.26	0.1896	0.1106
17.50	70.86	0.1909	0.1146
17.60	70.45	0.1923	0.1186
17.70	70.06	0.1936	0.1226
17.80	69.66	0.1948	0.1267
17.90	69.27	0.1958	0.1309
18.00	68.89	0.1965	0.1355

M. Ru_3Ta

λ/nm	$h\nu$/eV	δ	β
10.00	124.00	0.0402	0.0110
10.25	120.98	0.0428	0.0112
10.50	118.10	0.0456	0.0113
10.75	115.35	0.0484	0.0115
11.00	112.73	0.0516	0.0116
11.25	110.22	0.0549	0.0120
11.50	107.83	0.0585	0.0124
11.75	105.53	0.0622	0.0129
12.00	103.33	0.0661	0.0136
12.10	102.48	0.0677	0.0139
12.20	101.64	0.0694	0.0142
12.30	100.81	0.0709	0.0147
12.40	100.00	0.0726	0.0149
12.50	99.20	0.0743	0.0152
12.60	98.41	0.0760	0.0156
12.75	97.25	0.0787	0.0161
13.00	95.38	0.0835	0.0172
13.25	93.58	0.0886	0.0185
13.50	91.85	0.0940	0.0203
13.75	90.18	0.0996	0.0223
14.00	88.57	0.1053	0.0248
14.25	87.02	0.1112	0.0277
14.50	85.52	0.1170	0.0313
14.75	84.07	0.1226	0.0352
15.00	82.67	0.1283	0.0395
15.25	81.31	0.1340	0.0442
15.50	80.00	0.1393	0.0492
15.75	78.73	0.1446	0.0547
16.00	77.50	0.1497	0.0604
16.25	76.31	0.1548	0.0666
16.50	75.15	0.1596	0.0731
16.75	74.03	0.1645	0.0804
17.00	72.94	0.1687	0.0879
17.25	71.88	0.1728	0.0956
17.50	70.86	0.1757	0.1041
17.75	69.86	0.1784	0.1126
18.00	68.89	0.1811	0.1221
18.25	67.95	0.1826	0.1313
18.50	67.03	0.1836	0.1407
18.75	66.13	0.1824	0.1499
19.00	65.26	0.1807	0.1579
19.25	64.42	0.1786	0.1662
19.50	63.59	0.1768	0.1734
19.75	62.78	0.1729	0.1793
20.00	62.00	0.1727	0.1866

N. Ru_W

λ/nm	$h\nu$/eV	δ	β
10.00	124.00	0.0399	0.0122
10.10	122.77	0.0409	0.0123

(Table continued)

λ/nm	$h\nu$/eV	δ	β
10.20	121.57	0.0420	0.0124
10.30	120.39	0.0430	0.0124
10.40	119.23	0.0440	0.0124
10.50	118.10	0.0451	0.0123
10.60	116.98	0.0461	0.0123
10.70	115.89	0.0471	0.0122
10.80	114.81	0.0482	0.0123
10.90	113.76	0.0494	0.0124
11.00	112.73	0.0507	0.0125
11.10	111.71	0.0519	0.0126
11.20	110.71	0.0531	0.0126
11.30	109.73	0.0544	0.0126
11.40	108.77	0.0556	0.0126
11.50	107.83	0.0570	0.0127
11.60	106.90	0.0587	0.0130
11.70	105.98	0.0602	0.0131
11.80	105.08	0.0618	0.0133
11.90	104.20	0.0635	0.0135
12.00	103.33	0.0653	0.0138
12.10	102.48	0.0670	0.0140
12.20	101.64	0.0692	0.0146
12.30	100.81	0.0710	0.0154
12.40	100.00	0.0721	0.0149
12.50	99.20	0.0735	0.0147
12.60	98.41	0.0755	0.0151
12.70	97.64	0.0774	0.0155
12.80	96.88	0.0794	0.0159
12.90	96.12	0.0814	0.0164
13.00	95.38	0.0834	0.0169
13.10	94.66	0.0855	0.0174
13.20	93.94	0.0876	0.0180
13.30	93.23	0.0897	0.0187
13.40	92.54	0.0919	0.0194
13.50	91.85	0.0941	0.0201
13.60	91.18	0.0963	0.0209
13.70	90.51	0.0986	0.0218
13.80	89.86	0.1009	0.0227
13.90	89.21	0.1033	0.0237
14.00	88.57	0.1056	0.0247
14.10	87.94	0.1080	0.0258
14.20	87.32	0.1104	0.0270
14.30	86.71	0.1128	0.0283
14.40	86.11	0.1152	0.0296
14.50	85.52	0.1177	0.0310
14.60	84.93	0.1201	0.0325
14.70	84.35	0.1225	0.0341
14.80	83.78	0.1249	0.0357
14.90	83.22	0.1273	0.0374
15.00	82.67	0.1297	0.0392
15.10	82.12	0.1321	0.0411
15.20	81.58	0.1344	0.0429
15.30	81.05	0.1368	0.0449
15.40	80.52	0.1391	0.0469
15.50	80.00	0.1414	0.0490
15.60	79.49	0.1437	0.0510
15.70	78.98	0.1460	0.0532
15.80	78.48	0.1482	0.0554

(Table continued)

λ/nm	$h\nu$/eV	δ	β
15.90	77.99	0.1504	0.0577
16.00	77.50	0.1526	0.0601
16.10	77.02	0.1548	0.0626
16.20	76.54	0.1570	0.0651
16.30	76.07	0.1590	0.0678
16.40	75.61	0.1611	0.0705
16.50	75.15	0.1631	0.0733
16.60	74.70	0.1650	0.0763
16.70	74.25	0.1669	0.0793
16.80	73.81	0.1687	0.0824
16.90	73.37	0.1704	0.0855
17.00	72.94	0.1720	0.0888
17.10	72.51	0.1736	0.0920
17.20	72.09	0.1751	0.0954
17.30	71.68	0.1767	0.0989
17.40	71.26	0.1780	0.1023
17.50	70.86	0.1792	0.1058
17.60	70.45	0.1805	0.1095
17.70	70.06	0.1816	0.1132
17.80	69.66	0.1826	0.1169
17.90	69.27	0.1836	0.1207
18.00	68.89	0.1848	0.1248

O. RuTa

λ/nm	$h\nu$/eV	δ	β
10.00	124.00	0.0333	0.0165
10.25	120.98	0.0353	0.0168
10.50	118.10	0.0374	0.0171
10.75	115.35	0.0397	0.0174
11.00	112.73	0.0421	0.0177
11.25	110.22	0.0447	0.0181
11.50	107.83	0.0474	0.0186
11.75	105.53	0.0503	0.0191
12.00	103.33	0.0533	0.0196
12.10	102.48	0.0545	0.0197
12.20	101.64	0.0558	0.0201
12.30	100.81	0.0570	0.0204
12.40	100.00	0.0584	0.0206
12.50	99.20	0.0596	0.0209
12.60	98.41	0.0610	0.0212
12.75	97.25	0.0631	0.0217
13.00	95.38	0.0667	0.0226
13.25	93.58	0.0706	0.0237
13.50	91.85	0.0747	0.0249
13.75	90.18	0.0789	0.0264
14.00	88.57	0.0833	0.0281
14.25	87.02	0.0878	0.0302
14.50	85.52	0.0925	0.0324
14.75	84.07	0.0971	0.0351
15.00	82.67	0.1017	0.0381
15.25	81.31	0.1064	0.0414
15.50	80.00	0.1111	0.0449
15.75	78.73	0.1154	0.0489
16.00	77.50	0.1199	0.0529
16.25	76.31	0.1242	0.0575
16.50	75.15	0.1285	0.0625
16.75	74.03	0.1324	0.0683

(Table continued)

λ/nm	$h\nu$/eV	δ	β
17.00	72.94	0.1361	0.0739
17.25	71.88	0.1397	0.0799
17.50	70.86	0.1433	0.0862
17.75	69.86	0.1463	0.0926
18.00	68.89	0.1491	0.0998
18.25	67.95	0.1514	0.1066
18.50	67.03	0.1535	0.1140
18.75	66.13	0.1553	0.1205
19.00	65.26	0.1566	0.1277
19.25	64.42	0.1571	0.1359
19.50	63.59	0.1578	0.1426
19.75	62.78	0.1576	0.1506
20.00	62.00	0.1574	0.1570

P. $RuTa_3$

λ/nm	$h\nu$/eV	δ	β
10.00	124.00	0.0278	0.0219
10.25	120.98	0.0294	0.0221
10.50	118.10	0.0311	0.0224
10.75	115.35	0.0329	0.0227
11.00	112.73	0.0348	0.0232
11.25	110.22	0.0368	0.0236
11.50	107.83	0.0389	0.0241
11.75	105.53	0.0411	0.0246
12.00	103.33	0.0434	0.0251
12.10	102.48	0.0443	0.0253
12.20	101.64	0.0454	0.0256
12.30	100.81	0.0461	0.0261
12.40	100.00	0.0471	0.0262
12.50	99.20	0.0482	0.0265
12.60	98.41	0.0491	0.0267
12.75	97.25	0.0507	0.0271
13.00	95.38	0.0534	0.0278
13.25	93.58	0.0563	0.0285
13.50	91.85	0.0593	0.0295
13.75	90.18	0.0626	0.0305
14.00	88.57	0.0658	0.0317
14.25	87.02	0.0693	0.0330
14.50	85.52	0.0728	0.0344
14.75	84.07	0.0765	0.0360
15.00	82.67	0.0803	0.0378
15.25	81.31	0.0841	0.0399
15.50	80.00	0.0878	0.0421
15.75	78.73	0.0917	0.0446
16.00	77.50	0.0955	0.0472
16.25	76.31	0.0996	0.0502
16.50	75.15	0.1035	0.0533
16.75	74.03	0.1074	0.0568
17.00	72.94	0.1113	0.0604
17.25	71.88	0.1148	0.0640
17.50	70.86	0.1182	0.0682
17.75	69.86	0.1218	0.0726
18.00	68.89	0.1251	0.0771
18.25	67.95	0.1283	0.0818
18.50	67.03	0.1318	0.0873
18.75	66.13	0.1344	0.0925
19.00	65.26	0.1374	0.0983
19.25	64.42	0.1398	0.1040
19.50	63.59	0.1420	0.1101
19.75	62.78	0.1443	0.1163
20.00	62.00	0.1458	0.1228

Q. Ta

λ/nm	$h\nu$/eV	δ	β
10.00	124.00	0.0233	0.0259
10.25	120.98	0.0244	0.0264
10.50	118.10	0.0256	0.0269
10.75	115.35	0.0269	0.0274
11.00	112.73	0.0283	0.0279
11.25	110.22	0.0299	0.0283
11.50	107.83	0.0315	0.0288
11.75	105.53	0.0331	0.0294
12.00	103.33	0.0348	0.0300
12.10	102.48	0.0355	0.0302
12.20	101.64	0.0361	0.0305
12.30	100.81	0.0368	0.0307
12.40	100.00	0.0375	0.0310
12.50	99.20	0.0382	0.0313
12.60	98.41	0.0390	0.0315
12.75	97.25	0.0401	0.0318
13.00	95.38	0.0421	0.0324
13.25	93.58	0.0441	0.0329
13.50	91.85	0.0463	0.0335
13.75	90.18	0.0486	0.0341
14.00	88.57	0.0511	0.0348
14.25	87.02	0.0537	0.0355
14.50	85.52	0.0564	0.0364
14.75	84.07	0.0593	0.0373
15.00	82.67	0.0623	0.0383
15.25	81.31	0.0654	0.0394
15.50	80.00	0.0685	0.0406
15.75	78.73	0.0719	0.0420
16.00	77.50	0.0754	0.0435
16.25	76.31	0.0790	0.0451
16.50	75.15	0.0827	0.0470
16.75	74.03	0.0864	0.0490
17.00	72.94	0.0901	0.0513
17.25	71.88	0.0940	0.0538
17.50	70.86	0.0980	0.0564
17.75	69.86	0.1018	0.0592
18.00	68.89	0.1058	0.0623
18.25	67.95	0.1100	0.0657
18.50	67.03	0.1141	0.0693
18.75	66.13	0.1185	0.0732
19.00	65.26	0.1222	0.0775
19.25	64.42	0.1265	0.0820
19.50	63.59	0.1304	0.0870
19.75	62.78	0.1347	0.0921
20.00	62.00	0.1383	0.0978

R. TaBN

λ/nm	$h\nu$/eV	δ	β
10.00	124.00	0.0247	0.0234
10.10	122.77	0.0251	0.0237
10.20	121.57	0.0257	0.0238
10.30	120.39	0.0261	0.0239
10.40	119.23	0.0267	0.0239

(Table continued)

λ/nm	$h\nu$/eV	δ	β
10.50	118.10	0.0271	0.0241
10.60	116.98	0.0278	0.0242
10.70	115.89	0.0282	0.0243
10.80	114.81	0.0291	0.0245
10.90	113.76	0.0296	0.0248
11.00	112.73	0.0303	0.0248
11.20	110.71	0.0315	0.0250
11.30	109.73	0.0322	0.0252
11.40	108.77	0.0331	0.0256
11.50	107.83	0.0337	0.0263
11.60	106.90	0.0341	0.0260
11.70	105.98	0.0353	0.0264
11.80	105.08	0.0356	0.0264
11.90	104.20	0.0364	0.0268
12.00	103.33	0.0372	0.0271
12.10	102.48	0.0380	0.0273
12.20	101.64	0.0388	0.0277
12.30	100.81	0.0395	0.0280
12.40	100.00	0.0402	0.0283
12.50	99.20	0.0410	0.0285
12.60	98.41	0.0418	0.0289
12.70	97.64	0.0426	0.0291
12.80	96.88	0.0434	0.0294
12.90	96.12	0.0443	0.0298
13.00	95.38	0.0451	0.0301
13.10	94.66	0.0460	0.0304
13.20	93.94	0.0468	0.0307
13.30	93.23	0.0477	0.0310
13.40	92.54	0.0486	0.0314
13.50	91.85	0.0495	0.0318
13.60	91.18	0.0505	0.0321
13.70	90.51	0.0514	0.0325
13.80	89.86	0.0524	0.0329
13.90	89.21	0.0533	0.0332
14.00	88.57	0.0540	0.0335
14.10	87.94	0.0551	0.0338
14.20	87.32	0.0560	0.0342
14.30	86.71	0.0571	0.0346
14.40	86.11	0.0580	0.0350
14.50	85.52	0.0591	0.0353
14.60	84.93	0.0601	0.0357
14.70	84.35	0.0609	0.0360
14.80	83.78	0.0620	0.0364
14.90	83.22	0.0631	0.0367
15.00	82.67	0.0641	0.0371
15.10	82.12	0.0654	0.0376
15.20	81.58	0.0662	0.0379
15.30	81.05	0.0674	0.0384
15.40	80.52	0.0685	0.0389
15.50	80.00	0.0700	0.0392
15.60	79.49	0.0709	0.0397
15.70	78.98	0.0723	0.0403
15.80	78.48	0.0738	0.0407
15.90	77.99	0.0743	0.0410
16.00	77.50	0.0756	0.0418
16.10	77.02	0.0773	0.0422
16.20	76.54	0.0780	0.0428
16.30	76.07	0.0800	0.0434
16.40	75.61	0.0813	0.0440
16.50	75.15	0.0829	0.0445
16.60	74.70	0.0837	0.0453
16.70	74.25	0.0850	0.0462
16.80	73.81	0.0867	0.0469
16.90	73.37	0.0879	0.0473
17.00	72.94	0.0892	0.0483
17.10	72.51	0.0902	0.0487
17.30	71.68	0.0939	0.0506
17.40	71.26	0.0954	0.0514
17.50	70.86	0.0972	0.0525
17.60	70.45	0.0985	0.0531
17.70	70.06	0.1001	0.0542
17.80	69.66	0.1019	0.0554
17.90	69.27	0.1032	0.0562

(Table continued)

S. TaTeN

λ/nm	$h\nu$/eV	δ	β
10.00	124.00	0.0279	0.0115
10.20	121.57	0.0293	0.0126
10.40	119.23	0.0307	0.0138
10.60	116.98	0.0320	0.0153
10.80	114.81	0.0334	0.0169
11.00	112.73	0.0347	0.0188
11.20	110.71	0.0360	0.0209
11.40	108.77	0.0369	0.0232
11.60	106.90	0.0376	0.0255
11.80	105.08	0.0381	0.0280
12.00	103.33	0.0384	0.0304
12.20	101.64	0.0384	0.0326
12.40	100.00	0.0383	0.0346
12.60	98.41	0.0381	0.0365
12.80	96.88	0.0379	0.0382
13.00	95.38	0.0375	0.0399
13.20	93.94	0.0371	0.0416
13.40	92.54	0.0367	0.0431
13.60	91.18	0.0361	0.0445
13.80	89.86	0.0355	0.0457
14.00	88.57	0.0347	0.0466
14.20	87.32	0.0340	0.0474
14.40	86.11	0.0334	0.0482
14.60	84.93	0.0330	0.0487
14.80	83.78	0.0327	0.0495
15.00	82.67	0.0325	0.0503
15.20	81.58	0.0324	0.0510
15.40	80.52	0.0322	0.0521
15.60	79.49	0.0320	0.0525
15.80	78.48	0.0315	0.0537
16.00	77.50	0.0311	0.0546
16.20	76.54	0.0305	0.0550
16.40	75.61	0.0301	0.0552
16.60	74.70	0.0297	0.0553
16.80	73.81	0.0293	0.0557
17.00	72.94	0.0291	0.0558
17.20	72.09	0.0290	0.0556
17.40	71.26	0.0291	0.0558
17.60	70.45	0.0293	0.0554
17.80	69.66	0.0296	0.0551

S. TaTeN

λ/nm	$h\nu$/eV	δ	β
18.00	68.89	0.0301	0.0549
18.20	68.13	0.0308	0.0546
18.40	67.39	0.0317	0.0543
18.60	66.67	0.0327	0.0542
18.80	65.96	0.0337	0.0544
19.00	65.26	0.0348	0.0546
19.20	64.58	0.0359	0.0550
19.40	63.92	0.0369	0.0557
19.60	63.27	0.0380	0.0560
19.80	62.63	0.0391	0.0571

Funding. Horizon 2020 Framework Programme (20IND04, 662338, 783247).

Acknowledgment. We thank the engineers of the EUV radiometry group at PTB Berlin for their support during the measurements, especially Christian Laubis, Christian Buchholz, Christian Stadelhoff, Jana Puls, Heiko Mentzel, Anja Babuschkin, and Ayhan Babalik. The authors acknowledge that this project has received funding from the Electronic Component Systems for European Leadership Joint Undertaking under grant agreement 662338–SeNaTe and 783247–TAPES3, as well as from the EMPIR programme 20IND04 ATMOC. These Joint Undertakings receive support from the European Union's Horizon 2020 research and innovation program alongside the Netherlands, France, Belgium, Germany, Czech Republic, Austria, Hungary, and Israel.

Disclosures. The authors declare no conflicts of interest.

Data availability. Data underlying the results presented in this paper are not publicly available at this time but may be obtained from the authors upon reasonable request.

REFERENCES

1. V. Luong, V. Philipsen, E. Hendrickx, K. Opsomer, C. Detavernier, C. Laubis, F. Scholze, and M. Heyns, "Ni-Al alloys as alternative EUV mask absorber," Appl. Sci. **8**, 521 (2018).
2. V. Luong, V. Philipsen, K. Opsomer, J. Rip, E. Hendrickx, M. Heyns, C. Detavernier, C. Laubis, and F. Scholze, "Assessing stability of metal tellurides as alternative photomask materials for extreme ultraviolet lithography," J. Vac. Sci. Technol. B **37**, 061607 (2019).
3. M. Wu, D. Thakare, J.-F. de Marneffe, P. Jaenen, L. Souriau, K. Opsomer, J.-P. Soulié, A. Erdmann, H. Mesilhy, P. Naujok, M. Foltin, V. Soltwisch, Q. Saadeh, and V. Philipsen, "Study of novel EUVL mask absorber candidates," J. Micro/Nanopattern. Mater. Metrol. **20**, 021002 (2021).
4. M. Wu, J.-F. de Marneffe, K. Opsomer, C. Detavernier, A. Delabie, P. Naujok, Ö. Caner, A. Goodyear, M. Cooke, Q. Saadeh, V. Soltwisch, F. Scholze, and V. Philipsen, "Characterization of Ru(4-x)Ta(x) (x = 1, 2, 3) alloy as material candidate for EUV low-n mask," Micro Nano Eng. **12**, 100089 (2021).
5. B. Wu and A. Kumar, "Extreme ultraviolet lithography: a review," J. Vac. Sci. Technol. B **25**, 1743–1761 (2007).
6. B. Wu and A. Kumar, "Extreme ultraviolet lithography and three dimensional integrated circuit–a review," Appl. Phys. Rev. **1**, 011104 (2014).
7. J. S. Kim and J. Ahn, "Mask materials and designs for extreme ultra violet lithography," Electron. Mater. Lett. **14**, 533–547 (2018).
8. V. Bakshi, *EUV Lithography*, 2nd ed. (SPIE, 2018).
9. C. van Lare, F. Timmermans, and J. Finders, "Mask-absorber optimization: the next phase," J. Micro/Nanolithogr. MEMS MOEMS **19**, 1 (2020).
10. B. L. Henke, E. Gullikson, and J. Davis, "X-ray interactions: photoabsorption, scattering, transmission and reflection E = 50-30,000 eV, Z = 1-92," At. Data Nucl. Data Tables **54**, 181–342 (1993).
11. R. Soufli and E. M. Gullikson, "Optical constants of materials for multilayer mirror applications in the EUV/soft x-ray region," Proc. SPIE **3113**, 222–229 (1997).
12. L. G. Parratt, "Surface studies of solids by total reflection of X-rays," Phys. Rev. **95**, 359 (1954).
13. R. Müller, S. Yulin, P. Naujok, N. Kaiser, and A. Tünnermann, "Optical properties and oxidation resistance of different transition metals for soft x-ray and EUV applications," Thin Solid Films **624**, 1–6 (2017).
14. C. Tarrio, R. N. Watts, T. B. Lucatorto, J. M. Slaughter, and C. M. Falco, "Optical constants of in situ-deposited films of important extreme-ultraviolet multilayer mirror materials," Appl. Opt. **37**, 4100–4104 (1998).
15. H. Kiessig, "Untersuchungen zur totalreflexion von Röntgenstrahlen," Ann. Phys. (Berlin) **402**, 715–768 (1931).
16. M. Foster, M. Stamm, and G. Reiter, "X-ray reflectometer for study of polymer thin films and interfaces," Vacuum **41**, 1441–1444 (1990).
17. E. Chason and T. Mayer, "Thin film and surface characterization by specular x-ray reflectivity," Crit. Rev. Solid State Mater. Sci. **22**, 1–67 (1997).
18. M. Bass, C. DeCusatis, J. Enoch, V. Lakshminarayanan, G. Li, C. Macdonald, V. Mahajan, and E. Van Stryland, *Handbook of Optics*, 3rd ed. (McGraw-Hill, Inc., 2009), Vol. **I**: Geometrical and physical optics, polarized light, components and instruments.
19. L. Nevot and P. Croce, "Caractérisation des surfaces par réflexion rasante de rayons X. Application à l'étude du polissage de quelques verres silicates," Rev. Phys. Appl. **15**, 761–779 (1980).
20. G. Vignaud and A. Gibaud, "REFLEX: a program for the analysis of specular x-ray and neutron reflectivity data," J. Appl. Crystallogr. **52**, 201–213 (2019).
21. H. Fujiwara, *Spectroscopic Ellipsometry: Principles and Applications* (Wiley, 2007).
22. J. J. G. Perez and R. Ossikovski, *Polarized Light and the Mueller Matrix Approach* (CRC Press, 2016).
23. J. Jaiswal, S. Mourya, G. Malik, S. Chauhan, A. Sanger, R. Daipuriya, M. Singh, and R. Chandra, "Determination of optical constants including surface characteristics of optically thick nanostructured Ti films: analyzed by spectroscopic ellipsometry," Appl. Opt. **55**, 8368–8375 (2016).
24. F. Scholze, J. Tümmler, and G. Ulm, "High-accuracy radiometry in the EUV range at the PTB soft x-ray beamline," Metrologia **40**, S224 (2003).
25. F. Scholze, C. Laubis, C. Buchholz, A. Fischer, S. Ploeger, F. Scholz, H. Wagner, and G. Ulm, "Status of EUV reflectometry at PTB," Proc. SPIE **5751**, 749–758 (2005).
26. T. Uno and K. Hayashi, "Reflective mask blank for EUV lithography and process for producing the same," U.S. patent 8,956,787 B2 (February 17, 2015).
27. N. Koster, B. Mertens, R. Jansen, A. Van De Runstraat, F. Stietz, M. Wedowski, H. Meiling, R. Klein, A. Gottwald, F. Scholze, R. Vissere, M. Kurte, P. Zalme, E. Louis, and A. Yakshin, "Molecular contamination mitigation in EUVL by environmental control," Microelectron. Eng. **61**, 65–76 (2002).
28. C. Zhu, R. H. Byrd, P. Lu, and J. Nocedal, "Algorithm 778: L–BFGS–B: Fortran subroutines for large–scale bound–constrained optimization," ACM Trans. Math. Softw. **23**, 550–560 (1997).
29. R. Storn and K. Price, "Differential evolution–a simple and efficient heuristic for global optimization over continuous spaces," J. Global Optim. **11**, 341–359 (1997).
30. P. Virtanen, R. Gommers, T. E. Oliphant, M. Haberland, T. Reddy, D. Cournapeau, E. Burovski, P. Peterson, W. Weckesser, J. Bright, S. J. van der Walt, M. Brett, J. Wilson, K. J. Millman, N. Mayorov, A. R. J. Nelson, E. Jones, R. Kern, E. Larson, C. J. Carey, I. Polat, Y. Feng, E. W. Moore, J. VanderPlas, D. Laxalde, J. Perktold, R. Cimrman, I. Henriksen, E. A. Quintero, C. R. Harris, A. M. Archibald, A. H. Ribeiro, F. Pedregosa, and P. van Mulbregt, and SciPy 1.0 Contributors, "SciPy 1.0: fundamental algorithms for scientific computing in Python," Nat. Methods **17**, 261–272 (2020).
31. F. Grønvold, H. Haraldsen, and A. Kjekshus, "On the sulfides, selenides and tellurides of platinum," Acta Chem. Scand **14**, 1879–1893 (1960).
32. D. L. Windt, W. C. Cash, M. Scott, P. Arendt, B. Newnam, R. Fisher, and A. Swartzlander, "Optical constants for thin films of Ti, Zr, Nb,

Mo, Ru, Rh, Pd, Ag, Hf, Ta, W, Re, Ir, Os, Pt, and Au from 24 Å to 1216 Å," Appl. Opt. **27**, 246–278 (1988).
33. N. Pauly, F. Yubero, and S. Tougaard, "Optical properties of molybdenum in the ultraviolet and extreme ultraviolet by reflection electron energy loss spectroscopy," Appl. Opt. **59**, 4527–4532 (2020).
34. I. Diel, J. Friedrich, C. Kunz, S. Di Fonzo, B. Müller, and W. Jark, "Optical constants of float glass, nickel, and carbon from soft-x-ray reflectivity measurements," Appl. Opt. **36**, 6376–6382 (1997).
35. R. Soufli, F. Delmotte, J. Meyer-Ilse, F. Salmassi, N. Brejnholt, S. Massahi, D. Girou, F. Christensen, and E. M. Gullikson, "Optical constants of magnetron sputtered Pt thin films with improved accuracy in the N-and O-electronic shell absorption regions," J. Appl. Phys. **125**, 085106 (2019).
36. L. J. Bissell, D. D. Allred, R. S. Turley, W. R. Evans, and J. E. Johnson, "Determining ruthenium's optical constants in the spectral range 11–14 nm," Proc. SPIE **5538**, 84–91 (2004).
37. M. Hosoya, N. Sakaya, O. Nozawa, Y. Shiota, K. Hamamoto, O. Nagarekawa, S. Shimojima, T. Shoki, T. Watanabe, and H. Kinoshita, "Evaluating the optical index of Ta and Ta-based absorbers for an extreme ultraviolet mask using extreme ultraviolet reflectometry," Jpn. J. Appl. Phys. **47**, 4898 (2008).
38. L. V. Rodríguez-de Marcos, S. M. Kalaiselvi, O. B. Leong, P. K. Das, M. B. Breese, and A. Rusydi, "Optical constants and absorption properties of Te and TeO thin films in the 13-14 nm spectral range," Opt. Express **28**, 12922–12935 (2020).
39. C. T. Chantler, "Theoretical form factor, attenuation, and scattering tabulation for Z = 1–92 from E = 1–10 eV to E = 0.4–1.0 MeV," J. Phys. Chem. Ref. Data **24**, 71–643 (1995).
40. C. T. Chantler, "Detailed tabulation of atomic form factors, photoelectric absorption and scattering cross section, and mass attenuation coefficients in the vicinity of absorption edges in the soft X-ray (Z = 30–36, Z = 60–89, E = 0.1 keV–10 keV), addressing convergence issues of earlier work," J. Phys. Chem. Ref. Data **29**, 597–1056 (2000).
41. A. Andrle, P. Hönicke, J. Vinson, R. Quintanilha, Q. Saadeh, S. Heidenreich, F. Scholze, and V. Soltwisch, "The anisotropy in the optical constants of quartz crystals for soft x-rays," J. Appl. Cryst. **54**, 402–408 (2021).
42. J. T. Neumann, P. Gräupner, W. Kaiser, R. Garreis, and B. Geh, "Mask effects for high-NA EUV: impact of NA, chief-ray-angle, and reduction ratio," Proc. SPIE **8679**, 867915 (2013).
43. T. W. Barbee, S. Mrowka, and M. C. Hettrick, "Molybdenum-silicon multilayer mirrors for the extreme ultraviolet," Appl. Opt. **24**, 883–886 (1985).
44. J. Slaughter, D. W. Schulze, C. Hills, A. Mirone, R. Stalio, R. Watts, C. Tarrio, T. B. Lucatorto, M. Krumrey, P. Mueller, and C. M. Falco, "Structure and performance of Si/Mo multilayer mirrors for the extreme ultraviolet," J. Appl. Phys. **76**, 2144–2156 (1994).
45. S. Rizvi, *Handbook of Photomask Manufacturing Technology* (CRC Press, 2018).